Journal of Controlled Release 257 (2017) 60–67

Contents lists available at ScienceDirect

Journal of Controlled Release

journal homepage: www.elsevier.com/locate/jconrel

Cathepsin nanofiber substrates as potential agents for targeted drug delivery

Yael Ben-Nun [a], Galit Fichman [b], Lihi Adler-Abramovich [c], Boris Turk [d,e,f], Ehud Gazit [b,g], Galia Blum [a,*]

[a] The Institute for Drug Research, School of Pharmacy, Faculty of Medicine, Hebrew University, Jerusalem, Israel
[b] Department of Molecular Microbiology and Biotechnology, George S. Wise Faculty of Life Sciences, Tel Aviv University, Tel Aviv, Israel
[c] Department of Oral Biology, The Goldschleger School of Dental Medicine, Sackler Faculty of Medicine, Tel Aviv University, Tel Aviv, Israel
[d] Department of Biochemistry and Molecular Biology, J. Stefan Institute, Ljubljana, Slovenia
[e] Faculty of Chemistry and Chemical Technology, University of Ljubljana, Slovenia
[f] Centre of Excellence for Integrated Approaches in Chemistry and Biology of Proteins, Jamova cesta 39, SI-1000 Ljubljana, Slovenia
[g] Department of Materials Science and Engineering, Iby and Aladar Fleischman Faculty of Engineering, Tel Aviv University, Tel Aviv, Israel

ARTICLE INFO

Article history:
Received 8 September 2016
Received in revised form 19 November 2016
Accepted 24 November 2016
Available online 28 November 2016

Keywords:
Diphenylalanine
Self-assembly
Nanofibers
Cathepsins
Targeted drug delivery

ABSTRACT

The development of reactive drug carriers that could actively respond to biological signals is a challenging task. Different peptides can self-assemble into biocompatible nanostructures of various functionalities, including drugs carriers. Minimal building blocks, such as diphenylalanine, readily form ordered nanostructures. Here we present the development of self-assembled tetra-peptides that include the diphenylalanine motif, serving as substrates of the cathepsin proteases. This is of great clinical importance as cathepsins, whose activity and expression are highly elevated in cancer and other pathologies, have been shown to serve as efficient enzymes for therapeutic release. Based on the cathepsins affinity around the active site, we generated a library of Phe-Phe-Lys-Phe (FFKF) tetra-peptide substrates (TPSs). We inserted various N-termini capping groups with different chemical properties to investigate the effect on protease affinity and self-assembly. All nine TPSs were cleaved by their targets, cathepsins B and L. However, solvent switching led to nanofibers self-assembly of only seven of them. Due to its rapid self-assembly and complete degradation by cathepsin B, we focused on TPS4, Cbz-FFKF-OH. Degradation of TPS4 nanofibers by cathepsin B led to the release of 91.8 ± 0.3% of the incorporated anti-cancerous drug Doxorubicin from the nanofibers within 8 h while only 55 ± 0.2% was released without enzyme treatment. Finally, we demonstrated that tumor lysates fully degraded TPS4 nanofibers. Collectively, these results suggest that tetra-peptide substrates that form nanostructures could serve as a promising platform for targeted drug delivery to pathologies in which protease activity is highly elevated.

1. Introduction

To date, several drug delivery systems have been developed and applied overcoming both pharmacological limitations such as solubility, elimination half-life, stability and absorption, and pharmacodynamic difficulties such as specificity and low therapeutic index. Passive targeting of various nanoparticles like micelles and liposomes loaded with drugs have demonstrated great promise as drug-carriers utilizing the enhanced permeability retention (EPR) effect for delivery (for reviews, see [1–3]). In parallel, numerous groups have applied active targeting by decorating particles with targeting moieties such as receptor ligands [4], sugars [5], antibodies [6,7] and small molecule inhibitors [8].

The release of targeted drugs is often achieved by attaching the drug load to a carrier through specific peptide sequences which are cleaved by proteases that are highly expressed at the desired location. The peptide-drug conjugate can be created using hydrophobic or other non-covalent interactions, covalent modifications or as a part of a polymeric chain [9,10]. For example, drug-loaded liposomes and mesopores with short peptide targeting sequences have been introduced to enable drug release upon enzyme recognition and cleavage [11,12]. The cathepsin proteases thus often serve as the enzymes that release the drugs from their carrier.

Lysosomal cathepsins are a subfamily of cysteine proteases known to be involved in several processes of cancer progression such as tumor growth, invasion and metastasis [13,14]. Overexpression and activity of cathepsins B have been found in cancer as well as other pathologies, making them exceptional targets for precision therapeutics [14]. Tumor cell cathepsins are often secreted and translocate from their lysosomal location to the tumor microenvironment, providing an additional opportunity for targeting non-cell permeable therapeutics [8,15]. In particular,

* Corresponding author at: Institute for Drug Research, The School of Pharmacy, The Faculty of Medicine, The Hebrew University of Jerusalem, Jerusalem 9112001, Israel.
E-mail address: galiabl@ekmd.huji.ac.il (G. Blum).

http://dx.doi.org/10.1016/j.jconrel.2016.11.028
0168-3659/

cathepsin B has been found to be highly overexpressed and active in tumor associated macrophages (TAMs) making them a potential target for cancer immunotherapy [16]. An essential component of substrate specificity of cathepsins, as in other proteases, is recognition of the sequence around the scissile (cleaved) bond within the substrate. Many studies have revealed cathepsin proteases affinity for positively charged amino acids at the P1 site and bulky hydrophobic amino acids at the P2 and P3 sites [17–19]. A recent example of a cathepsin substrate that meets the above criteria is the Cbz-Phe-Lys that has been used by several groups for targeting of therapeutics and imaging reagents [18,20–25].

The use of short peptide sequences for nanotechnology and nanomedicine has recently gained popularity due to their biodegradability, simple preparation, reproducibility, and ability to spontaneously form 3D structures [26–28]. The most prominent are hydrophobic peptide building blocks that can self-assemble into well-organized nanostructures [29–32]. The process of self-assembly can be induced by different triggers such as enzymatic catalysis [33], light induction [34], or changes in temperature [35], pH [36,37] or solvent [38,39]. The simplest and most widely studied of these building blocks are the Phe-Phe (FF) variants whose self-assembly is mostly governed by hydrophobic and aromatic π-π stacking interactions [40,41]. Due to their lack of toxicity, FF nanostructures are highly biocompatible and therefore used for biological applications. Recently, FF nanostructures have been reported in several biological systems for applications in 3D cell culture [42,43], bio-imaging [44], biosensors [32,45] and drug delivery, where FF nanostructures, known to undergo endocytosis, were applied for transporting oligonucleotides and small molecules to intracellular destinations [46,47].

The popularity of the FF motif for biological applications together with the known cathepsin affinity for hydrophobic amino acids encouraged us to design a self-assembly cathepsin tetra-peptide substrate (TPS) for therapeutic delivery. We reasoned that a short peptide sequence that contains di-aromatic and a positively charged amino acid could serve as a potential cathepsin substrate and simultaneously allow for self-assembly. Therefore, we explored a variety of Phe-Phe-Lys-Phe (FFKF) analogs as self-assembled cathepsin substrates to be used as carriers with specific drug release properties.

2. Results and discussion

To target the delivery of therapeutics to cancerous tissues with elevated cathepsin activity, we designed a series of TPSs based on the FFKF scaffold. To optimize the TPSs self-assembly our peptide designs contain unique N-termini chemical groups and charge variation at the C-termini (Scheme 1a). Aromatic chemical groups were introduced at the N- and C-termini to ensure that the addition of the Lys to the FF variant will not impair the self-assembly process. Following synthesis of these peptides (Scheme S1), we studied their ability to be recognized and cleaved by cathepsin proteases. The peptides were incubated with either cathepsin B or cathepsin L and their cleavage products were analyzed using mass spectroscopy (MS). A tri-peptide fragment FFK was the expected cleavage product since the target site for cleavage by these cathepsins is

postulated to be the amide bond after the P1 Lys, recognized by the protease S1 pocket (Scheme 1b) [17–19,48]. Results obtained from MS analysis revealed that all TPSs were recognized and cleaved by both enzymes. In addition to the expected tri-peptide cleavage product, di-peptides and/or single amino acids were detected (Fig. 1), as accounted for by the known highly promiscuous nature of the cathepsin proteases [49]. It is widely accepted that the sequence determines the substrate specificity to a protease, in some cases we found correlations between the cleavage pattern and the peptide N-termini capping group. In cathepsin B for example, a charged amine group led to removal of a single amino acid while bulky hydrophobic groups (Fmoc or Cbz) led to removal of two or three amino acids.

Next, we investigated the ability of the different TPSs to self-assemble into ordered nanostructures using a solvent-mediated approach to trigger the assembly [50,51]. Nanostructures formation was verified by transmission electron microscopy (TEM), revealing that all TPSs self-assembled into ordered structures with morphology of elongated nanofibers network, excluding TPS6 and 7 (Fig. 2 and Supplementary Fig. S1). In most cases the addition of a charged amino acid, Lys, to the fundamental FF structure did not prohibit structure formation, most likely because of the many aromatic rings within the TPSs. We observed variance in the nanofibers diameters of the different TPSs (Table S1) that we attribute to the chemical modifications at the N- and C-termini. Aromatic moieties (such as Fmoc and Cbz) and carbonyl/amide groups (Scheme 1) can contribute to the total π-π and hydrogen bond interactions, respectively. These additional interactions may enable stronger stacking forces yielding “well-packed” nanostructures with relatively smaller diameter [52]. Interestingly, upon assembly initiation TPS4 stood out since it instantly formed fibers, while most other TPSs took over 2 h to assemble, as was confirmed by microscopic examination (data not shown).

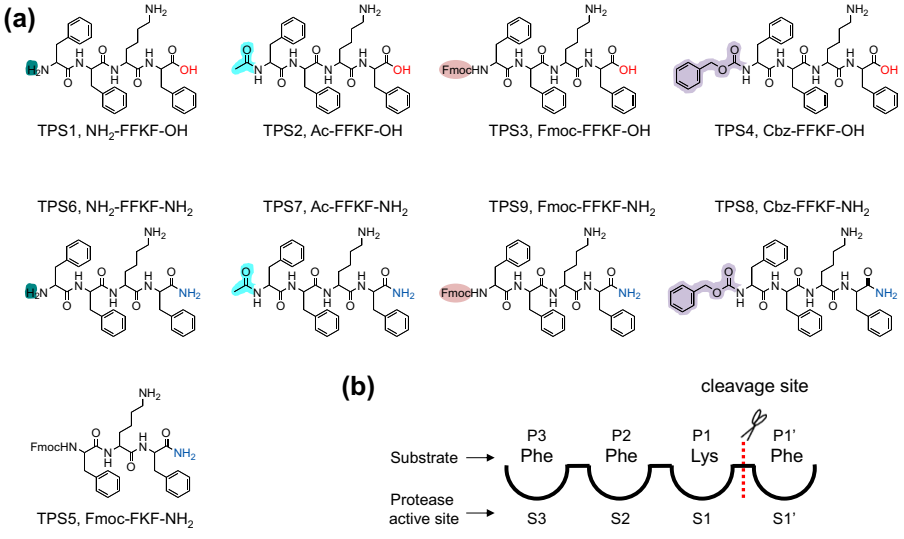

Scheme 1. Structures of TPSs. (a) Pairs of TPSs were designed based on the FFKF scaffold, each pair carrying a unique N-termini chemical group and a variation in the C-termini charge. Carboxyl group is marked in red and amide group in blue. (b) Protease-substrate standard notation, protease binding pockets (S) and corresponding substrate amino acid (P). The cleavage site is the scissile bond between the *P*1 (N-termini to the scissile bond) and *P*1′ (C-termini to the scissile bond) residues. Adopted from Schechter and Berger [47].

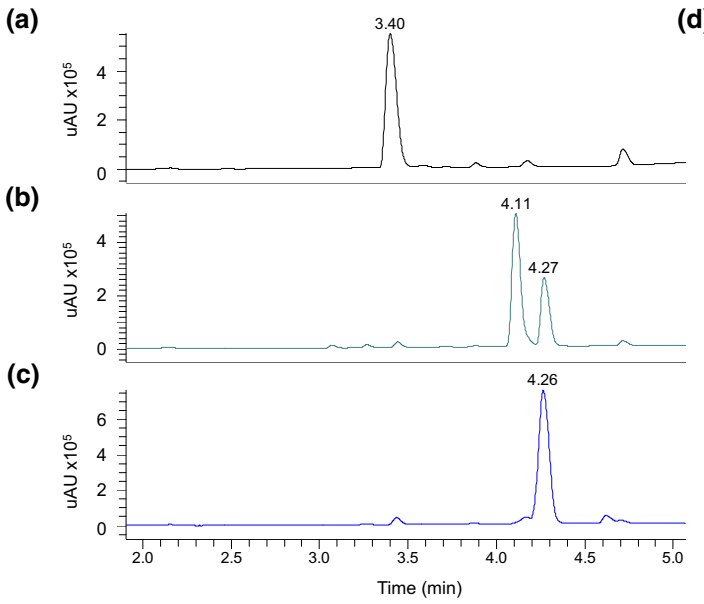

(d) Number of amino acids removed after cathepsin treatment

	Cat B	Cat L
TPS1 NH_2-FFKF-OH	1	2
TPS2 Ac-FFKF-OH	2	2
TPS3 Fmoc-FFKF-OH	2, 3	2
TPS4 Cbz-FFKF-OH	2	2
TPS5 Fmoc-FKF-amide	1	1
TPS6 NH_2-FFKF-amide	1	2
TPS7 Ac-FFKF-amide	1	2
TPS8 Cbz-FFKF-amide	ND*	2
TPS9 Fmoc-FFKF-amide	2, 3	1, 2

Fig. 1. TPS cleavage by cathepsins. Each TPS was treated with cathepsin B, cathepsin L or vehicle at 37 °C. Cleavage products were analyzed by liquid chromatography-MS (LC-MS). Representative HPLC chromatograms of TPS3 absorbance at 215 nm is shown (a) TPS3, (b) TPS3 after cathepsin B treatment, (c) TPS3 after cathepsin L treatment. (d) A table showing the number of amino acids removed from each TPS after cathepsin treatment, according to the fragment analysis by LC-MS. Cat; cathepsin, ND; not determined, * detected fragments identity could not be determined.

Considering its immediate self-assembly, we decided to continue with TPS4 (Cbz-FFKF-OH), as a self-assembling peptide-substrate model for cleavage by cathepsin B. TPS4 was found to assemble into ordered nanofibers, forming an opaque peptide-solution upon assembly initiation. To evaluate the assembly kinetics of TPS4 we examined the turbidity changes of the self-assembled peptide at different peptide concentrations by monitoring the absorbance at 350 nm. Absorbance was already detected at the initial time point followed by a significant increase in turbidity during the first 5 h (Supplementary Fig. S2) indicating continuous assembly of the nanofibers over the course of the experiment. This increase in turbidity is in line with the recent report of the assembly of Boc-Phe-Phe, where nanofibers formation was associated with the increase in turbidity [53]. Upon addition of cathepsin B to the assembled TPS4 a decrease in turbidity was obtained, due to the degradation of the nanofibers by the enzyme (Fig. 3a). To validate that the decrease in turbidity was a result of nanofiber degradation, samples of nanofibers with and without cathepsin B treatment were analyzed by TEM at the final time point. While very few nanofibers were found in the samples treated with cathepsin B, a substantial number of nanofibers were easily found in non-treated samples (Supplementary Fig. S3). This validated that cathepsin B can access TPS4 and degrade it even as assembled nanofibers.

We further evaluated nanofiber degradation by cathepsin B at various TPS4 concentrations to examine the optimum peptide concentration for best assembly and degradation when the assembly process reached equilibrium. As expected, under the tested conditions a significant and robust degradation of TSP4 assemblies was obtained for all tested peptide concentrations. Most dramatic turbidity reduction was found at the lowest concentration tested, 0.5 mg/ml. At the higher TPS concentration, however, only partial degradation was

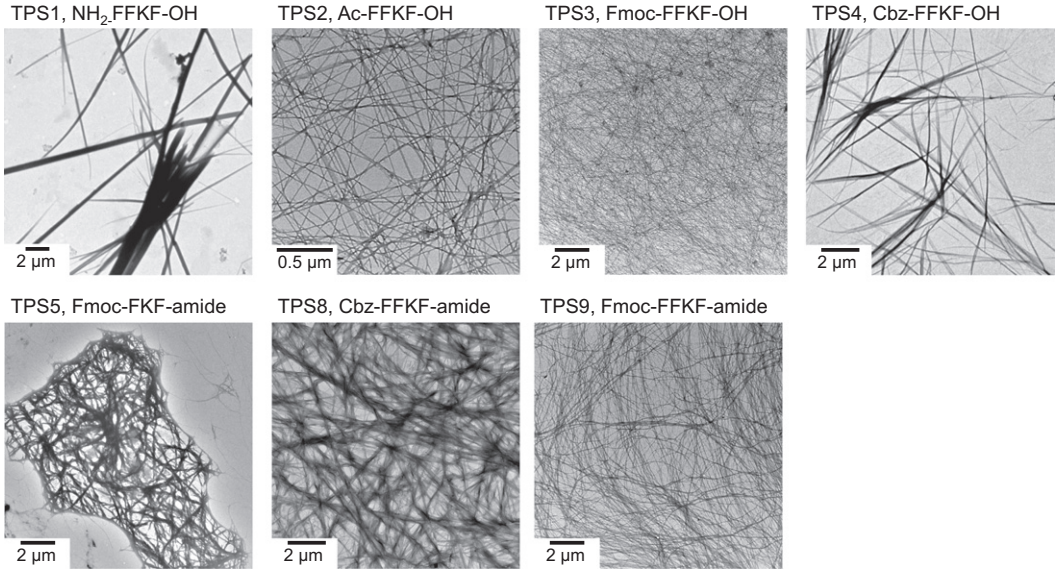

Fig. 2. TPS self-assembly. The self-assembly of various TPSs was triggered by solvent-switching between DMSO and water. Final concentration of 5 mg/ml of TPS1, 2, and 1 mg/ml of TPS3-5, 8 and 9 were analyzed. TEM analysis revealed self-assembled nanofibers with different morphologies for all TPSs, excluding TPS6 and 7.

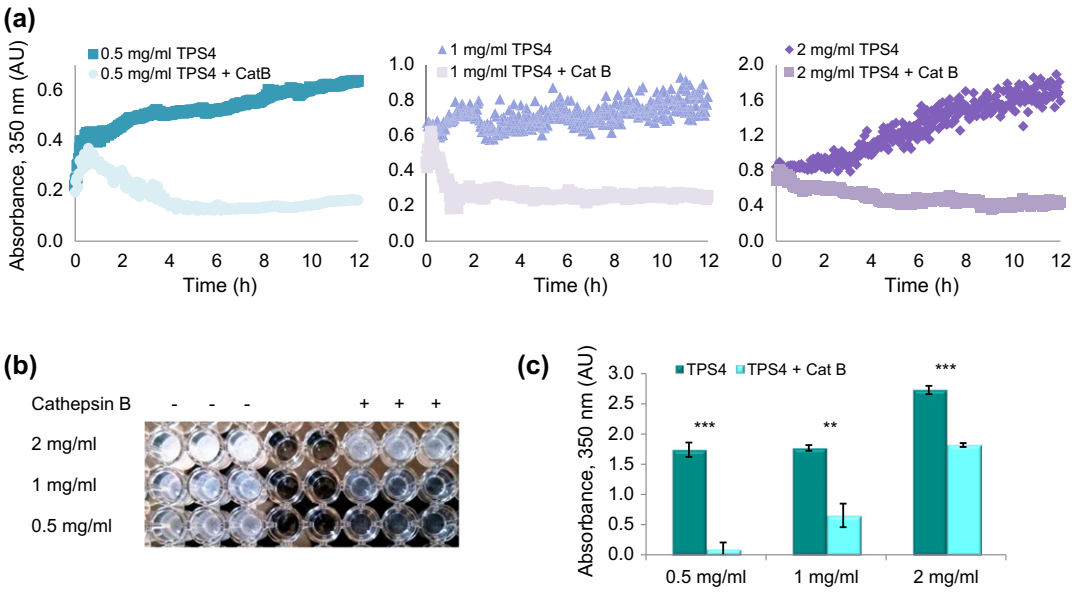

Fig. 3. TPS4 nanofibers degradation by cathepsin B. (a) Following assembly of TPS4 at the indicated peptide concentrations, cathepsin B or vehicle were added. The degradation of the assembled TPS4 was evaluated by turbidity measurements monitoring the absorbance at 350 nm. Addition of cathepsin B led to decreased turbidity due to enzyme-mediated degradation of the nanofibers. (b) A representative image of TPS4 assembly at different concentrations with (right) and without (left) cathepsin B treatment. Samples treated with cathepsin B show higher transparency. (c) Quantification of absorbance at 350 nm from (b) indicating the significant reduction in turbidity in cathepsin B treated samples. Results described with standard deviation, ** $p < 0.01$, *** $p < 0.001$.

observed (Fig. 3b and c). We speculate that at higher peptide concentrations more assemblies are present in the solution that might physically limit the accessibility of the enzyme to the substrate. Another possibility is that the degradation products are quickly recovered and assembled to the remaining TPS structures that are present at a high concentration in the surrounding environment. Overall these results suggest that nanofibers degradation is concentration dependent and that TPS4 assemblies should be optimized to generate suitable drug delivery systems.

To further investigate the ability of TPS4 to serve as a cathepsin targeted drug delivery vehicle we first evaluated growth inhibition by TPS4 and found no cytotoxicity of MDA-MB 231 cells by 0.5 mg/ml (Supplementary Fig. 4). Then we assessed the ability of assemblies obtained from 0.5 mg/ml TPS4 to serve as a carrier for the anti-cancerous drug Doxorubicin (Dox). Dox was chosen as a model drug because of its intrinsic fluorescent properties which allow easy monitoring of the drug. Initially, Dox was encapsulated in nanofibers of TPS4 by solvent switching of the mixture from DMSO to water, generating fluorescent

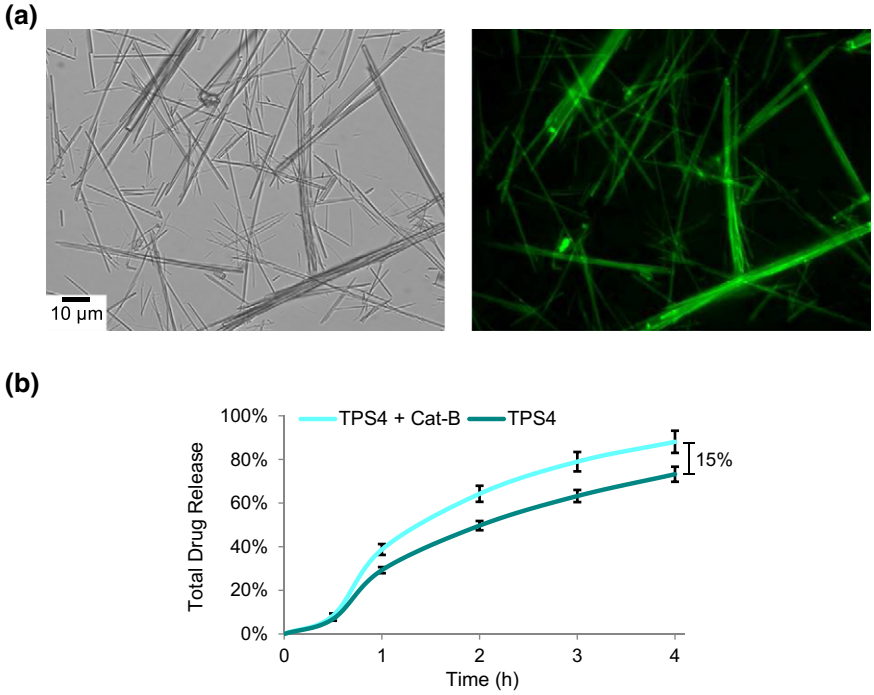

Fig. 4. TPS4 nanofibers as a targeted drug-release carrier. (a) The assembly of premixed solution of Dox and TPS4 in DMSO was triggered by solvent change and allowed for overnight self-assembly in the dark. Bright field (left) and fluorescent microscopy (excitation 535 ± 50 nm, emission 610 ± 75 nm) (right). (b) Cathepsin B or vehicle were added to samples from (a) and released drug was collected for 4 h by dialysis. Amount of released Dox was extrapolated from a fluorescent Dox calibration curve, results described with standard deviation.

nanofibers as visualized by fluorescent microscopy (Fig. 4a). Exposure of the Dox containing nanofibers to cathepsin B resulted in drug release due to nanofibers degradation. Unfortunately, we found only a 15% difference in the release profile when comparing the amount of drug released from the nanofibers with or without the enzyme (Fig. 4b). We suspected that Dox was only coating the nanofibers by weak interactions and was spontaneously released thus leading to the small differences observed upon enzyme addition.

To improve the release profile upon enzyme treatment, we attempted to first generate small Dox particles and then coat them with peptide nanofibers. The Dox particles were inspired by the doxil liposome in which drug retention was achieved by base change of a weak-base-drug with sulfate ions in an intra-liposome aqueous phase. In that process, after accumulation in a liposome filled with ammonium sulfate, $(doxorubicin)_2SO_4$ (doxorubicin sulfate) precipitated [54]. To investigate our hypothesis, we first generated Dox particles (DPs) by precipitation with ammonium sulfate and then coated these particles with peptide nanofibers triggering the assembly of TPS4 by solvent exchange, Dox loading efficiency was found to be 48 ± 5%. The new assembly, Dox particles-TPS4 (DP-TPS4), formed highly fluorescence structures, as observed by fluorescent microscopy (Fig. 5a and b). Scanning electron microscopy (SEM) and TEM analysis of the DPs revealed differences in the structures formed with and without TPS4. DPs alone formed unstructured aggregates as well as fibers with 10–20 nm diameter (Fig. 5c and d, marked by a white arrow). DPs-TPS4 formed defined nanofibers throughout, with fibers diameter ranging from 40 to 60 nm (Fig. 5e and f). We then turned to investigate the release profile of Dox from DP-TPS4 assemblies in the presence or absence of cathepsin B. As expected, in the presence of the enzyme a significant increase in Dox release was obtained that reached 91.8 ± 0.3% after 8 h, as compared to the spontaneous, non-specific, drug release from DPs-TPS4 structures without enzyme treatment (55.0 ± 0.2%), (Fig. 5g).

Recently we analyzed the expression and activity levels of cathepsins in 4T1 murine breast cancer cells [20]. Similar to other cancers, this cell line naturally expresses high levels of various cathepsins, especially cathepsin B. Therefore, we evaluated the ability of 4T1 tumor lysates from tumor-bearing mice to degrade TPS4 nanofibers. We found that the tumor lysates degraded TPS4 nanofibers in a concentration-dependent manner (Supplementary Fig. 5). We then evaluated TPS4 nanofiber degradation over time by tissue lysates, while 4T1 tumor lysates degraded the majority of TPS4 nanofibers within 2 h, the lysates generated from mice muscles had limited effect in the first 10 h tested, (Fig. 6). Taking these results together, we foresee that tetra-peptide substrates that form nanostructures could serve as a promising platform for targeted drug delivery to cancers that exhibit highly elevated protease activities.

3. Conclusions

In conclusion, we applied a substrate-based approach to generate a library of self-assembled tetra-peptides to serve as carriers for therapeutics to pathological tissues characterized by elevated protease activity. We have demonstrated that in most cases elongation of the FF variant by two additional amino acids, including a charged lysine, did not impair the self assembly of substrates into ordered nanofibers. Furthermore, we show the capability of the cathepsin proteases to process their substrates both in solution and within nanostructures. Generation of Dox particles-TPS4 led to an improved release profile of Dox from the nanostructures by cathepsin B activity. Finally, we demonstrated that the intrinsic high cathepsin activity of tumor lysates can fully degrade

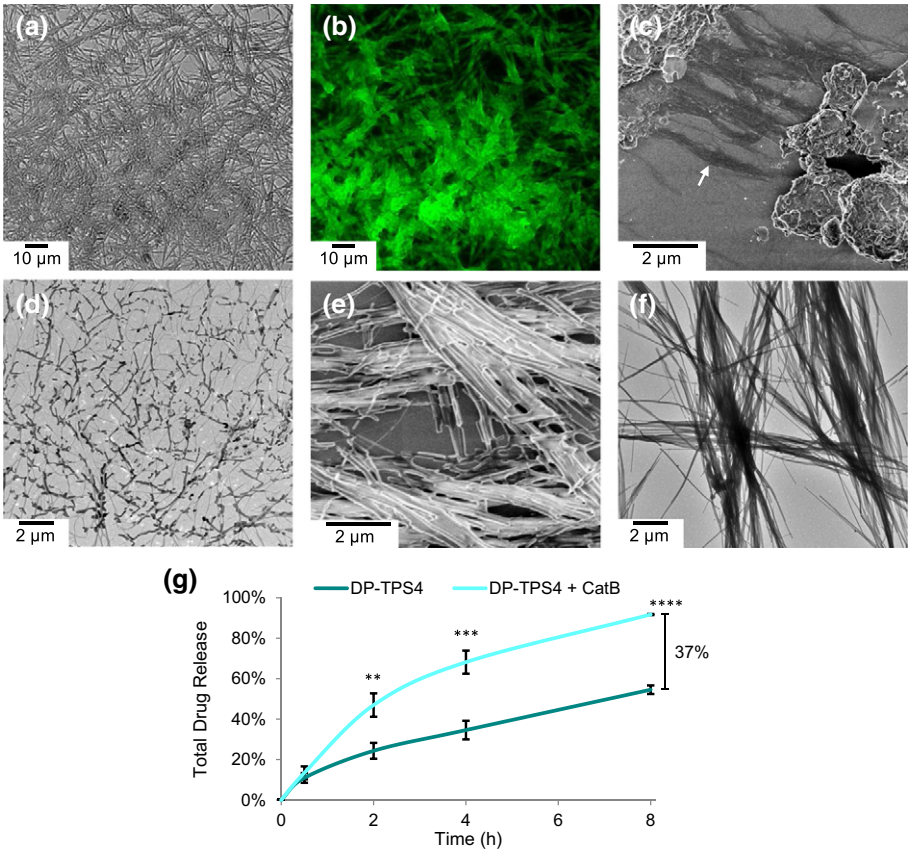

Fig. 5. Improved drug release profile. Dox was precipitated by ammonium sulfate to generate Dox particles (DPs), TPS4 was added and allowed to assemble overnight. Bright field (a) and fluorescent microscopy of DP-TPS4 (b). Analysis of DPs alone forming unstructured aggregates as well as fibers (white arrow), SEM (c) and TEM (d). Analysis of DPs-TPS4 showing defined nanofibers by SEM (e) and TEM (f). Release profile of Dox from DP-TPS4 nanostructure in the presence and absence of cathepsin B, as described in Fig. 4b (g). After 8 h 91.8 ± 0.3% of total drug was released from DP-TPS4 following cathepsin B treatment. Results are described with standard error, ** $p < 0.01$, *** $p < 0.001$, **** $p < 0.0001$.

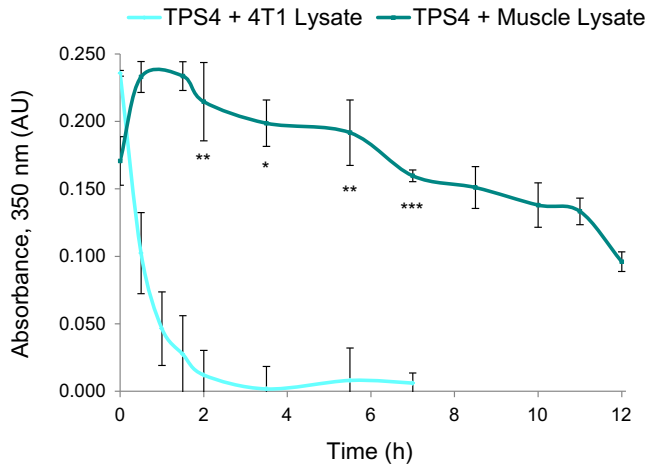

Fig. 6. TPS4 nanofibers degradation by tissue lysates. Following 0.5 mg/ml TPS4 assembly, lysates from 4T1 tumors or from mice muscles were added and the degradation of the assembled TPS4 was evaluated by turbidity measurements, monitoring the absorbance at 350, nm. Addition of 4T1 tumor lysates led to dramatic decreased turbidity resulting from enzyme-mediated degradation of the nanofibers. Results described with standard error, * $p < 0.05$, ** $p < 0.01$, *** $p < 0.001$.

TPS4 nanofibers. Our findings suggest a new platform for drug-delivery, targeted to pathologies with high cathepsins activity.

4. Materials and methods

4.1. Chemical synthesis

Unless otherwise noted, all resins and reagents were purchased from commercial suppliers and used without further purification. Tetra peptides were synthesis on solid phase using 2-Chlorotrityl chloride resin (peptide 1-5) or Rink-amide resin (peptide 6-9) with Fmoc based chemistry. Peptide elongation was performed with 1-hydroxybenzotriazole (HOBT) and (benzotriazole-1-yl oxy) tripyrrolidinophosphonium hexafluorophosphate (PyBOP) as coupling reagents and diisopropylethylamine (DIEA). Cleavage of peptide from the resin and t-butyloxycarbonyl (Boc) deprotection were performed using trifluoroacetic acid (TFA) in dichloro methane (DCM). Peptides were purified by C18 reverse phase HPLC in acetonitrile/water gradient supplemented with 0.1% TFA or by precipitation. Final peptides were characterized by a Liquid Chromatography Mass Spectrometer (LCMS) - Thermo Scientific MSQ-Plus attached to an Accela UPLC system to >95% purity. Final peptides were lyophilized and kept at −20 °C until use.

4.2. Cleavage of substrate peptides by cathepsins

Each peptide (1 nmole) was treated with 0.9 μmol cathepsin B or cathepsin L (generated as described in [55,56]) or acetate buffer vehicle (50 mM acetate, 5 mM $MgCl_2$, 2 mM DTT, adjusted to pH 5.5) for 3 h at 37 °C. Next, enzymes were precipitated by an hour incubation at −80 °C in 80% cold methanol followed by 10 min of 6000 *g* centrifugation at 4 °C. Supernatant volume was reduced to about 15 μl under vacuum, adjusted to a final volume of 30 μl with methanol and analyzed by LCMS equipped with C18 reverse phase.

4.3. Assembly preparation

Lyophilized peptides were dissolved in DMSO to a concentration of 100 mg/ml and then diluted in double-distilled water (DDW) to the indicated final concentration.

4.4. Transmission electron microscopy analysis

Transmission electron microscopy (TEM) analysis was performed by applying 10 μl of samples to a 200 or 400-mesh copper grids covered by carbon-stabilized Formvar film (SPI, West Chester, PA). The samples were allowed to adsorb for 2 min before excess fluid was blotted off. Samples were negatively stained by depositing 10 μl of 2% uranyl acetate on the grid and allowing it to adsorb for 2 min before excess fluid was blotted off. Except the sample in Fig. 5e, all samples were negatively stained. TEM micrographs were recorded using a JEOL 1200EX or JEOL JEM-1400Plus electron microscope operating at different kV.

4.5. Scanning electron microscopy

Scanning Electron Microscopy (SEM) samples were prepared as described above for TEM on a 400-mesh copper grids, without uranyl acetate staining, and viewed using FEI Magellan™ 400L system.

4.6. Kinetics of TPS4 self-assembly

Freshly prepared aliquots of 0.5, 1 or 2 mg/ml of TPS4 were placed in triplicates in a 96-well plate, 100 μl/well. Plate was placed at 37 °C in a Biotek Cytation 3 plate reader (Winooski, VT, USA) and absorbance at 350 nm was measured every 2 min during 5 h.

4.7. Turbidity analysis of TPS4 degradation by cathepsin B

Turbidity analysis for TPS4 solutions was conducted using triplicates of freshly prepared solutions as described above in a 96 well plate. Aliquots of 1, 2 or 4 mg/ml were allowed to assemble for 4–5 h at room temperature. Next, 0.064, 0.128 or 0.255 μM of cathepsin B or acetate buffer vehicle were added, diluting the samples to 0.5, 1, and 2 mg/ml, respectively. The plate was placed at 37 °C in a Biotek Synergy HT plate reader (Winooski, VT, USA) and absorbance was measured for 12 h as described above. After 24 h since enzyme addition, a color picture was taken and the turbidity was measured again.

4.8. TPS4 nanofibers cytotoxicity

MDA-MB 231 human breast adenocarcinoma cells were cultured in Dulbecco's modified eagle's medium (DMEM) supplemented with 10% fetal bovine serum (FBS), 1% penicillin and 1% streptomycin in a humidified atmosphere of 5% CO_2 at 37 °C. One day prior to treatment MDA-MB 231 cells (7×10^3 cells/well) were cultured in a 96-well plate. The media of TPS4 that was assembled in DMEM was removed by centrifugation (14,000 rpm, 4 °C) and the nanofibers were resuspended in DMEM supplemented with 10% FBS, 1% penicillin and 1% streptomycin. Cells in triplicates were incubated with 0.5 mg/ml of TPS4 nanofibers (final concentration of 0.1% DMSO was kept constant) in growth medium at 37 °C. After 24 or 48 h of treatment, cell survival was determined by standard methylene blue assay. This assay was performed twice.

4.9. TPS4 assembly in the presence of Dox

Assembly of TPS4 in the presence of Dox was achieved by premixing the peptide and the drug in DMSO followed by a dilution in DDW to final concentration of 1 mg/ml TPS4 and 5% *w*/w Dox. The assembly was preformed over-night in the dark. Next, access of Dox were washed off by centrifugation (10 min, 14,000 rpm or 5 min, 8200 rpm, 4 °C respectively) and the resulting Dox containing nanofibers were resuspended in DDW to a final concentration of 1 mg/ml. For fluorescent characterization, 5 ml of each assembly were placed on a coverslip and allowed for complete dryness in the dark. Fluorescent images were taken at 60 x magnification using an Olympus inverted fluorescent microscope IX51 equipped with a TritC filter (ex/em 535 ± 50/610 ± 75 nm). This experiment was performed at least three times.

4.10. Preparation of DP

Doxorubicin·HCl (Sigma Aldrich), 1.06 mg, was dissolved in 2 μl dry DMSO. Then, 69 μl of 20 mM ammonium sulfate aqueous solution were added followed by a short sonication. DP were precipitated by 10 min centrifugation at 14,000 rpm, 4 °C to obtain a red pellet and a light red supernatant. Supernatant was removed and re-precipitated by ammonium sulfate aqueous solution. Pellets were combined and resuspended in DDW to a final concentration of 10 mg/ml DP. This experiment was performed at least three times.

4.11. DP-TPS4 assembly

Assembly of TPS4 in the presence of DP was achieved by dilution while stirring of TPS4 in a solution of DP suspended in 20 mM ammonium sulfate. The assembly was preformed overnight in the dark. Next, access of Dox or DP were washed off by centrifugation (10 min, 14,000 rpm or 5 min, 8200 rpm, 4 °C respectively) and the resulting DP-TPS4 was resuspended in DDW to a final concentration of 1 mg/ml. Fluorescent characterization was performed as in 4.9. This experiment was performed at least three times.

4.12. Determination of Dox loading in DP-TPS4

Following DP-TPS4 assembly as described above, the supernatant of access Dox was collected by centrifugation (10 min, 14,000 rpm, 4 °C) and the resulting precipitation of DP-TPS4 was dissolved in DMSO. Dox fluorescence intensity in supernatant and precipitation was read at excitation/emission of 480/595 nm by a Cytation 3 plate reader and the amount of Dox was obtained from the calibration curve of Dox in 20 mM ammonium sulfate or DMSO respectively. The loading efficiency of DP in DP-TPS4 assembly was determined by the ratio of amount obtained from DP-TPS4 precipitation to the total amount obtained from supernatant and DP-TPS4 precipitation. Loading efficiency was determined in triplicates, this experiment was performed three times.

4.13. Release of Dox by cathepsin B

20% *w*/w DP or 5% *w*/w Dox in 1 mg/ml assembly (as described above) were placed in a dialysis unit (1 kDa molecular weight cut-off, Slide-A-Lyzer™ MINI Dialysis Devices, Thermo Fisher Scientific). Next, cathepsin B was added to generate a final concentration of 0.5 mg/ml nanofibers assembly and 2 μM cathepsin B. The samples were placed at 37 °C and dialyzed while gently shaking, with dialysis replaced at indicated time points. At the end of the experiment, samples in dialysis units were collected and recovered. All collected samples were lyophilized and resuspended in DMSO and the fluorescence intensity of Dox was read at excitation/emission of 480/595 nm by a Cytation 3 plate reader. The amount of released Dox was obtained from the calibration curve of Dox in DMSO. This experiment in triplicate was performed three times.

4.14. Kinetics of nanofibers degradation by tissue lysates

Tissue lysates were prepared as previously described [20]. Assembly of TPS4 in triplicates was performed for 4 h in acetate buffer as described in Fig. 3b. Next, 100 μg of lysates from 4T1 tumor or muscles, or RIPA vehicle control (1% Tergitol-type NP-40 (nonyl phenoxypolyethoxylethanol), 0.1% SDS, 0.5% sodium deoxycholate) were added in acetate buffer. The absorbance was read at 350 nm after gentle shaking at 37 °C for indicated times using a BioTek plate reader. This experiment was performed twice.

Author contributions

The manuscript was written through contributions of all authors. All authors have given approval to the final version of the manuscript.

Funding sources

This work was supported by grants from the Israeli National Nanotechnology Initiative and Helmsley Charitable Trust (ISL008) for a focal technology area on nanomedicines for personalized theranostics (Galia Blum and Ehud Gazit) and by a grant from Slovene Research Agency (P1-0140) (Boris Turk).

Acknowledgments

Authors would like to thank Avraham J. Domb, Darya Tsvirkun, Emma Portnoy and Seth J. Saltpeter from the School of Pharmacy, the Hebrew University for fruitful discussions, Eduard Berenshtein from the electron microscopy lab of the Hebrew University Core Research Facility for aiding in TEM analysis, Inna Popov, The Unit for Nanocharacterization, Hebrew University for SEM analysis.

Appendix A. Supplementary data

Supplementary data to this article can be found online at http://dx.doi.org/10.1016/j.jconrel.2016.11.028.

References

[1] T.M. Allen, P.R. Cullis, Liposomal drug delivery systems: from concept to clinical applications, Adv. Drug Deliv. Rev. 65 (2013) 36–48.
[2] J. Gong, M. Chen, Y. Zheng, S. Wang, Y. Wang, Polymeric micelles drug delivery system in oncology, J. Control. Release 159 (2012) 312–323.
[3] U. Kedar, P. Phutane, S. Shidhaye, V. Kadam, Advances in polymeric micelles for drug delivery and tumor targeting, Nanomed. Nanotechnol. Biol. Med. 6 (2010) 714–729.
[4] S. Ni, S.M. Stephenson, R.J. Lee, Folate receptor targeted delivery of liposomal daunorubicin into tumor cells, Anticancer Res. 22 (2002) 2131–2135.
[5] B.G. Davis, M.A. Robinson, Drug delivery systems based on sugar-macromolecule conjugates, Curr. Opin. Drug Discov. Dev. 5 (2002) 279–288.
[6] P.F. Bross, J. Beitz, G. Chen, X.H. Chen, E. Duffy, L. Kieffer, S. Roy, R. Sridhara, A. Rahman, G. Williams, R. Pazdur, Approval summary: gemtuzumab ozogamicin in relapsed acute myeloid leukemia, Clin. Cancer Res. 7 (2001) 1490–1496.
[7] K.V. Foyil, N.L. Bartlett, Brentuximab vedotin for the treatment of CD30+ lymphomas, Immunotherapy 3 (2011) 475–485.
[8] G. Mikhaylov, D. Klimpel, N. Schaschke, U. Mikac, M. Vizovisek, M. Fonovic, V. Turk, B. Turk, O. Vasiljeva, Selective targeting of tumor and stromal cells by a nanocarrier system displaying lipidated cathepsin B inhibitor, Angew. Chem. Int. Ed. Eng. 53 (2014) 10077–10081.
[9] M.J. Vicent, F. Greco, R.I. Nicholson, A. Paul, P.C. Griffiths, R. Duncan, Polymer therapeutics designed for a combination therapy of hormone-dependent cancer, Angew. Chem. Int. Ed. Eng. 44 (2005) 4061–4066.
[10] R. Satchi, T.A. Connors, R. Duncan, PDEPT: polymer-directed enzyme prodrug therapy. I. HPMA copolymer-cathepsin B and PK1 as a model combination, Br. J. Cancer 85 (2001) 1070–1076.
[11] M.T. Basel, T.B. Shrestha, D.L. Troyer, S.H. Bossmann, Protease-sensitive, polymer-caged liposomes: a method for making highly targeted liposomes using triggered release, ACS Nano 5 (2011) 2162–2175.
[12] N. Singh, A. Karambelkar, L. Gu, K. Lin, J.S. Miller, C.S. Chen, M.J. Sailor, S.N. Bhatia, Bioresponsive mesoporous silica nanoparticles for triggered drug release, J. Am. Chem. Soc. 133 (2011) 19582–19585.
[13] V. Gocheva, W. Zeng, D. Ke, D. Klimstra, T. Reinheckel, C. Peters, D. Hanahan, J.A. Joyce, Distinct roles for cysteine cathepsin genes in multistage tumorigenesis, Genes Dev. 20 (2006) 543–556.
[14] J.A. Joyce, A. Baruch, K. Chehade, N. Meyer-Morse, E. Giraudo, F.Y. Tsai, D.C. Greenbaum, J.H. Hager, M. Bogyo, D. Hanahan, Cathepsin cysteine proteases are effectors of invasive growth and angiogenesis during multistage tumorigenesis, Cancer Cell 5 (2004) 443–453.
[15] M.M. Mohamed, B.F. Sloane, Cysteine cathepsins: multifunctional enzymes in cancer, Nat. Rev. Cancer 6 (2006) 764–775.
[16] V. Gocheva, H.W. Wang, B.B. Gadea, T. Shree, K.E. Hunter, A.L. Garfall, T. Berman, J.A. Joyce, IL-4 induces cathepsin protease activity in tumor-associated macrophages to promote cancer growth and invasion, Genes Dev. 24 (2010) 241–255.
[17] Y. Choe, F. Leonetti, D.C. Greenbaum, F. Lecaille, M. Bogyo, D. Bromme, J.A. Ellman, C.S. Craik, Substrate profiling of cysteine proteases using a combinatorial peptide library identifies functionally unique specificities, J. Biol. Chem. 281 (2006) 12824–12832.

[18] D. Bromme, A. Steinert, S. Friebe, S. Fittkau, B. Wiederanders, H. Kirschke, The specificity of bovine spleen cathepsin S. A comparison with rat liver cathepsins L and B, Biochem. J. 264 (1989) 475–481.
[19] V. Turk, V. Stoka, O. Vasiljeva, M. Renko, T. Sun, B. Turk, D. Turk, Cysteine cathepsins: from structure, function and regulation to new frontiers, Biochim. Biophys. Acta Proteins Proteomics 1824 (2012) 68–88.
[20] Y. Ben-Nun, E. Merquiol, A. Brandis, B. Turk, A. Scherz, G. Blum, Photodynamic quenched cathepsin activity based probes for cancer detection and macrophage targeted therapy, Theranostics 5 (2015) 847–862.
[21] G. Blum, S.R. Mullins, K. Keren, M. Fonovic, C. Jedeszko, M.J. Rice, B.F. Sloane, M. Bogyo, Dynamic imaging of protease activity with fluorescently quenched activity-based probes, Nat. Chem. Biol. 1 (2005) 203–209.
[22] G.M. Dubowchik, R.A. Firestone, L. Padilla, D. Willner, S.J. Hofstead, K. Mosure, J.O. Knipe, S.J. Lasch, P.A. Trail, Cathepsin B-labile dipeptide linkers for lysosomal release of doxorubicin from internalizing immunoconjugates: model studies of enzymatic drug release and antigen-specific in vitro anticancer activity, Bioconjug. Chem. 13 (2002) 855–869.
[23] E. Kisin-Finfer, S. Ferber, R. Blau, R. Satchi-Fainaro, D. Shabat, Synthesis and evaluation of new NIR-fluorescent probes for cathepsin B: ICT versus FRET as a turn-ON mode-of-action, Bioorg. Med. Chem. Lett. 24 (2014) 2453–2458.
[24] K. Miller, R. Erez, E. Segal, D. Shabat, R. Satchi-Fainaro, Targeting bone metastases with a bispecific anticancer and antiangiogenic polymer-alendronate-taxane conjugate, Angew. Chem. Int. Ed. Eng. 48 (2009) 2949–2954.
[25] L.P. Sadowski, P.E. Edem, J.F. Valliant, A. Adronov, Synthesis of polyester dendritic scaffolds for biomedical applications, Macromol. Biosci. (2016) (n/a-n/a).
[26] U.O. Seker, H.V. Demir, Material binding peptides for nanotechnology, Molecules 16 (2011) 1426–1451.
[27] R. de la Rica, H. Matsui, Applications of peptide and protein-based materials in bionanotechnology, Chem. Soc. Rev. 39 (2010) 3499–3509.
[28] S. Marchesan, A.V. Vargiu, K.E. Styan, The Phe-Phe motif for peptide self-assembly in nanomedicine, Molecules 20 (2015) 19775–19788.
[29] P.W.J.M. Frederix, R.V. Ulijn, N.T. Hunt, T. Tuttle, Virtual screening for dipeptide aggregation: toward predictive tools for peptide self-assembly, J. Phys. Chem. Lett. 2 (2011) 2380–2384.
[30] D.J. Adams, Dipeptide and tripeptide conjugates as low-molecular-weight hydrogelators, Macromol. Biosci. 11 (2011) 160–173.
[31] A.V. Vargiu, D. Iglesias, K.E. Styan, L.J. Waddington, C.D. Easton, S. Marchesan, Design of a hydrophobic tripeptide that self-assembles into amphiphilic superstructures forming a hydrogel biomaterial, Chem. Commun. 52 (2016) 5912–5915.
[32] M. Yemini, M. Reches, J. Rishpon, E. Gazit, Novel electrochemical biosensing platform using self-assembled peptide nanotubes, Nano Lett. 5 (2005) 183–186.
[33] S. Toledano, R.J. Williams, V. Jayawarna, R.V. Ulijn, Enzyme-triggered self-assembly of peptide hydrogels via reversed hydrolysis, J. Am. Chem. Soc. 128 (2006) 1070–1071.
[34] L.A. Haines, K. Rajagopal, B. Ozbas, D.A. Salick, D.J. Pochan, J.P. Schneider, Light-activated hydrogel formation via the triggered folding and self-assembly of a designed peptide, J. Am. Chem. Soc. 127 (2005) 17025–17029.
[35] S. Debnath, A. Shome, D. Das, P.K. Das, Hydrogelation through self-assembly of fmoc-peptide functionalized cationic amphiphiles: potent antibacterial agent, J. Phys. Chem. B 114 (2010) 4407–4415.
[36] Y. Wang, S. Yi, L. Sun, Y. Huang, S.C. Lenaghan, M. Zhang, Doxorubicin-loaded cyclic peptide nanotube bundles overcome chemoresistance in breast cancer cells, J. Biomed. Nanotechnol. 10 (2014) 445–454.
[37] A.M. Smith, R.J. Williams, C. Tang, P. Coppo, R.F. Collins, M.L. Turner, A. Saiani, R.V. Ulijn, Fmoc-diphenylalanine self assembles to a hydrogel via a novel architecture based on π–π interlocked β-sheets, Adv. Mater. 20 (2008) 37–41.
[38] G. Fichman, L. Adler-Abramovich, S. Manohar, I. Mironi-Harpaz, T. Guterman, D. Seliktar, P.B. Messersmith, E. Gazit, Seamless metallic coating and surface adhesion of self-assembled bioinspired nanostructures based on di-(3.4-dihydroxy-L-phenylalanine) peptide motif, ACS Nano 8 (2014) 7220–7228.
[39] G. Fichman, E. Gazit, Self-assembly of short peptides to form hydrogels: design of building blocks, physical properties and technological applications, Acta Biomater. 10 (2014) 1671–1682.
[40] M. Reches, E. Gazit, Casting metal nanowires within discrete self-assembled peptide nanotubes, Science 300 (2003) 625–627.
[41] C.H. Gorbitz, The structure of nanotubes formed by diphenylalanine, the core recognition motif of Alzheimer's beta-amyloid polypeptide, Chem. Commun. (Camb.) (2006) 2332–2334.
[42] V. Jayawarna, M. Ali, T.A. Jowitt, A.F. Miller, A. Saiani, J.E. Gough, R.V. Ulijn, Nanostructured hydrogels for three-dimensional cell culture through self-assembly of Fluorenylmethoxycarbonyl–dipeptides, Adv. Mater. 18 (2006) 611–614.
[43] A. Mahler, M. Reches, M. Rechter, S. Cohen, E. Gazit, Rigid, self-assembled hydrogel composed of a modified aromatic dipeptide, Adv. Mater. 18 (2006) 1365–1370.
[44] X. Yan, Y. Cui, W. Qi, Y. Su, Y. Yang, Q. He, J. Li, Self-assembly of peptide-based colloids containing lipophilic nanocrystals, Small 4 (2008) 1687–1693.
[45] M. Yemini, M. Reches, E. Gazit, J. Rishpon, Peptide nanotube-modified electrodes for enzyme-biosensor applications, Anal. Chem. 77 (2005) 5155–5159.
[46] X. Yan, Q. He, K. Wang, L. Duan, Y. Cui, J. Li, Transition of cationic dipeptide nanotubes into vesicles and oligonucleotide delivery, Angew. Chem. Int. Ed. Eng. 46 (2007) 2431–2434.
[47] J. Li, Y. Gao, Y. Kuang, J. Shi, X. Du, J. Zhou, H. Wang, Z. Yang, B. Xu, Dephosphorylation of D-peptide derivatives to form biofunctional, supramolecular nanofibers/hydrogels and their potential applications for intracellular imaging and intratumoral chemotherapy, J. Am. Chem. Soc. 135 (2013) 9907–9914.
[48] I. Schechter, A. Berger, On the size of the active site in proteases. I. Papain, Biochem. Biophys. Res. Commun. 27 (1967) 157–162.
[49] V. Turk, B. Turk, D. Turk, Lysosomal cysteine proteases: facts and opportunities, EMBO J. 20 (2001) 4629–4633.
[50] G. Fichman, T. Guterman, L. Adler-Abramovich, E. Gazit, Synergetic functional properties of two-component single amino acid-based hydrogels, CrystEngComm 17 (2015) 8105–8112.
[51] D.M. Ryan, S.B. Anderson, F.T. Senguen, R.E. Youngman, B.L. Nilsson, Self-assembly and hydrogelation promoted by F5-phenylalanine, Soft Matter 6 (2010) 475–479.
[52] M. Reches, E. Gazit, Self-assembly of peptide nanotubes and amyloid-like structures by charged-termini-capped diphenylalanine peptide analogues, Isr. J. Chem. 45 (2005) 363–371.
[53] L. Adler-Abramovich, P. Marco, Z.A. Arnon, R.C. Creasey, T.C. Michaels, A. Levin, D.J. Scurr, C.J. Roberts, T.P. Knowles, S.J. Tendler, E. Gazit, Controlling the physical dimensions of peptide nanotubes by supramolecular polymer coassembly, ACS Nano 5 (2016) 5.
[54] Y. Barenholz, Doxil(*R*)–the first FDA-approved nano-drug: lessons learned, J. Control. Release 160 (2012) 117–134.
[55] J. Rozman, J. Stojan, R. Kuhelj, V. Turk, B. Turk, Autocatalytic processing of recombinant human procathepsin B is a bimolecular process, FEBS Lett. 459 (1999) 358–362.
[56] M. Mihelic, A. Dobersek, G. Guncar, D. Turk, Inhibitory fragment from the p41 form of invariant chain can regulate activity of cysteine cathepsins in antigen presentation, J. Biol. Chem. 283 (2008) 14453–14460.